Body Sculpting

13

Marc J. Salzman

Abstract

HRUS is most useful to plastic surgeons in the surveillance of the integrity of silicone gel breast implants. HRUS is also being used to facilitate the diagnosis and aspiration seromas of the breast and abdomen. Reconstructive plastic surgeons have found HRUS useful in the planning of fasciocutaneous flap surgeries. This chapter explores how HRUS can help esthetically enhance plastic surgery procedures and help the procedures in their accuracy.

Keywords

HRUS · Breast implants · Fat grafting · Brazilian Buttock Lift · Fillers · Nerve block · Cellulite

13.1 Introduction

Plastic surgeons have been one of the last medical specialties to embrace the use of ultrasound in the care of their patients. High-resolution linear probes with frequencies in the 7–13 MHz range are commonly used for both diagnostic and therapeutic plastic surgical applications. The advent of portable ultrasound devices with acquisition costs in the $2000–$ 12,000 range have made the addition of high-resolution ultrasound (HRUS) more available to plastic surgeons. Wireless HRUS devices, which can more easily be used intraoperatively, have made it easier for plastic surgeons to utilize ultrasound to improve the accuracy of procedures such as fat grafting and the "Brazilian Buttock Lift."

13.2 HRUS for Breast Implants

One of the most commonly performed reconstructive or cosmetic plastic surgery procedures involves the placement of silicone gel breast implants. According to the American Society of Plastic Surgeons 2018 Plastic Surgery Statistics report, there were 101,657 breast reconstructions and 313,735 cosmetic breast augmentations performed in 2018 [1]. Breast implants all contain a silicone elastomer shell and can be filled with either saline or silicone gel (Fig. 13.1).

The vast majority of breast implants contain a single lumen or chamber. Other breast implant types that are clinically encountered have a dual lumen construct with either saline on the inside chamber and silicone gel within the outer or the reverse. These dual lumen breast implants allow for intraoperative adjustability of the size of the implant. The silicone elastomer can have either a textured or smooth surface (Fig. 13.2).

M. J. Salzman (✉)
Plastic Surgery, University of Louisville, Louisville, KY, USA
e-mail: mjs@itbecomesyou.com

R. L. Bard (ed.), *Image-Guided Aesthetic Treatments*, https://doi.org/10.1007/978-3-031-36266-8_13

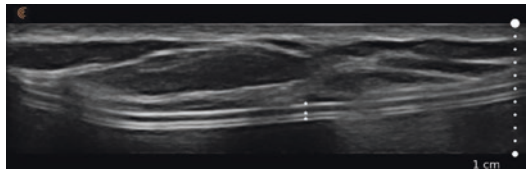

Fig. 13.1 Grayscale ultrasound image of smooth silicone gel breast implant. Top * represents the capsule surrounding the breast implant. The bottom pair of * represent the elastomer shell of the breast implant

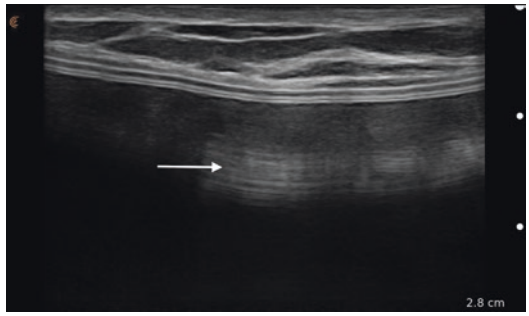

Fig. 13.2 Grayscale ultrasound image of smooth silicone gel breast implant. Arrow shows reverberation artifact of implant elastomer shell

The thickness of the silicone elastomer shell varies from less than a millimeter to just over 2 mm. Almost all silicone gel breast implants are formed over a dome-shaped mandrel and are filled with silicone gel through an opening on the posterior surface of the implant. This posterior opening is covered with a thicker segment of a silicone patch that is glued to the surface of the shell during the last stages of the manufacturing process. A relative newcomer to the choice in breast implant construction is the structured saline implant (Ideal Implant, Dallas, Texas) (Fig. 13.3).

A structured saline implant contains two saline filled chambers and a series of internal implant shells nested together. Breast implants can be round or shaped. Modern breast implants are made with varying height to base width ratios allowing for multiple choices to meet the needs of a myriad of anatomical corrections. Breast implants can be placed below the pectoralis major muscle (submuscular), below the fascia overlying the pectoralis major muscle (subfascial) or above the fascia of the pectoralis major muscle

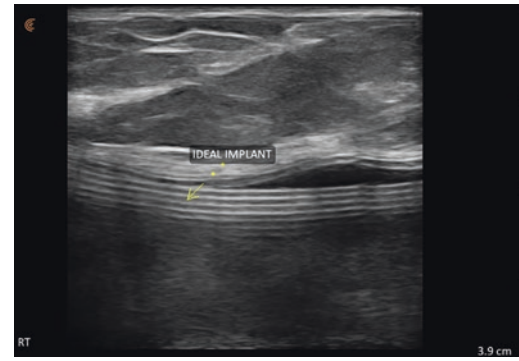

Fig. 13.3 Grayscale ultrasound image of a structured saline implant (Ideal implant, Dallas, Texas) showing a shell within a shell configuration

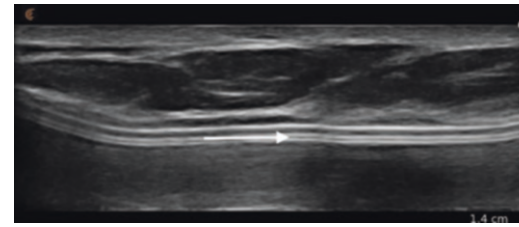

Fig. 13.4 Grayscale ultrasound image of smooth silicone gel breast implant. Arrow depicts the elastomer shell with smooth contour

(subglandular). Common access incisions for placement of breast implants include the inframammary crease, periareolar margin, axilla, and umbilicus. After the placement of breast implants, the body forms a fibrous capsule around the implant. Breast implants have been used since the 1960s [2]. Early generation silicone gel breast implants had very thin elastomeric shells and a honey-like internal gel consistency. The unpolymerized silicone gel could leak through the implant shell and migrate into the surrounding breast capsule (silicone gel bleed). Because of the high rupture rate of this type of implant, later generations of silicone gel implants have an internal barrier to gel diffusion and have a thicker gel consistency due to the higher amount of cross-linked silicone. Breast implant manufacturers have an array of breast implant softness or "feel" that the implant can have based on the ratio of polymerized to unpolymerized gel (Figs. 13.4 and 13.5).

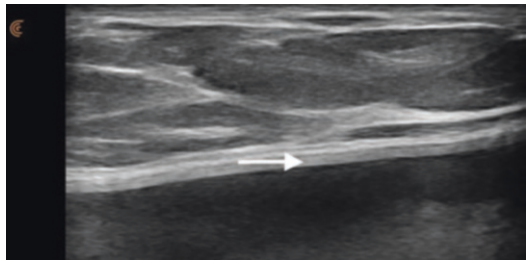

Fig. 13.5 Grayscale ultrasound image of textured silicone gel breast implant. Arrow depicts the elastomer shell with fuzzy contour

Higher cross-linked amounts of silicone cause a firmer feel. Newer, 5th generation silicone gel breast implants are all classified as containing a cohesive gel or "gummy bear" consistency. The failure rate of silicone breast implants has been described [3–5]. Symptoms of silicone breast implant rupture can include capsular contracture, distortion of implant shape, neurogenic pain, a palpable lump, or an axillary mass. Many of the silicone gel breast implant failures are "silent," and the patient has no symptoms and no visible or palpable changes on physical exam. In 1992, because of a suspicion of a relationship between silicone gel breast implants and autoimmune disease, a moratorium was placed by the U.S. Food and Drug Administration (FDA) on the use of silicone gel breast implants for breast augmentation [6]. This decision was reversed in 2006 [7]. One of the concerns of the FDA was the detection of "silent rupture" of silicone gel breast implants. For that reason, the FDA recommended that patients having silicone gel breast implants have an MRI at 3 years post implantation and every 2 years thereafter [8]. MRI is costly and inconvenient for surveillance of the integrity of silicone breast implants. At the FDA General and Plastic Surgery Panel in March 2019, the American College of Radiology reported on the ACR Appropriateness Criteria that MRI for asymptomatic women with silicone gel breast implants is not recommended and that consideration should be made for recommendation of later and less often screening with ultrasound [9]. The ability of ultrasound to diagnose rupture of silicone gel breast implants has been compared in the literature to MRI and mammography [10–14]. Because of the inability of mammography to visualize the internal aspects of the silicone gel breast implant, the sensitivity of mammography in detecting silicone gel breast implant rupture reported at a range of 11–69% is higher for extracapsular rupture [15–19]. The reported sensitivity of ultrasound for the detection of a rupture of a silicone gel breast implant is reported at a range of 30–75% [10, 12–14, 18, 20]. Ultrasound is more likely to correctly predict when a silicone gel breast implant is intact with reported negative predictive values of 50–90% [21].

With lower cost, convenience, and availability within the plastic surgeons' office, ultrasound is a better first screening tool in examining the plastic surgery breast implant patient than an MRI. An economic analysis of screening tests for the detection of ruptured silicone gel breast implants done at the University of Michigan suggested that considering the costs and diagnostic accuracy of ultrasound compared to MRI, it was concluded that initial screening with ultrasound followed by MRI was best in asymptomatic patients, and ultrasound was the preferred screening modality in symptomatic women [22].

13.3 The Breast Implant Exam

It may be useful prior to beginning the ultrasound evaluation of breast implants to inquire what type of breast implant was placed. Occasionally, the patient might retain the breast implant card provided to them at the time of their surgery with the information about the manufacturing company, size, type, shape, and volume of their implants. After multiple prior breast implant surgeries, the patient's recollection of the implant specifics may be unreliable. The patient lays in the supine position with the arm over her head. A high-frequency linear probe, 7–15 MHz, is used to scan all four quadrants of the breast. Slightly lower frequencies in the 5–7.5 MHz range may be used for larger breasts and to better image the posterior portion of the breast implant. Attempt is made to scan with the probe oriented transversely with the angle of ultrasound beam directed

perpendicular to the surface of the shell/capsule interface. When examining the surface of the breast implant, depth of the scan is superficial such that the shell/capsule interface lies in the near field to increase visualization of small imperfections in the shell. Depth can then be increased to best visualize the posterior surface of the implant along the chest wall. Breast implants with suggested pathology such as folds or loss of continuity of the elastomer shell should have compression images and videos taken with pressure applied from the opposite side of the imaging quadrant in attempt to unfurl the fold or visualize separation of the shell at the sight of discontinuity. The ability of the sonologist to manipulate the image with pressure application is one of the advantages of ultrasound over the static image achieved by MRI. The lateral border of the pectoralis major muscle and axilla should be scanned for lymph nodes containing silicone.

13.4 The Normal Silicone Breast Implant

In the unbroken, single lumen silicone gel breast implant, the double-line echogenic elastomer shell is seen just below the echogenic fibrous capsule. This creates the normal trilaminar line seen in the unbroken silicone breast implant. The outermost echogenic line corresponds to the breast implant capsule. The middle echogenic line is a fusion of the inner aspect of the breast capsule and the outer aspect of the breast implant elastomer shell. The innermost echogenic line represents the inner aspect of the elastomer shell [23]. A small amount of fluid with some mild echogenicity can usually be seen between the fibrous breast capsule and the elastomer shell of the implant. Textured surface implants will sometimes have more of this normal fluid interface than a smooth walled device. Breast implant placement can be under the gland (subglandular), below the pectoralis major muscle (subpectoral), or less frequently below the fascia of the pectoralis major (subfascial). The inferior aspect of the subpectoral breast implant will extend below the inferior border of the pectoralis muscle and lie above the rectus abdominis and serratus fascias but below the breast gland. The periprosthetic breast implant capsule can be located below or above the pectoralis muscle depending upon the plane of implant placement and position of ultrasound probe relative to the inferior border of the pectoralis muscle. Inside the unbroken, normal implant, just below the elastomer shell, reverberation artifact is represented by echogenic parallel lines seen below the shell. In comparison to the "subcapsular sign" representing collapse of a portion the elastomer shell into the gel of the interior of the implant, the reverberation artifact echogenic lines seen below the elastomer shell of the implant tend to be parallel to the shell, of similar length to each other and fairly evenly spaced apart from each other [24]. Often, these artifactual echogenic lines can be reduced in the image with application of less pressure on the transducer over the implant. The remaining interior of the implant appears mostly anechoic. The anterior and side aspects of the implant shell can usually be visualized. The posterior wall of the implant may be difficult to assess. Ultrasound images of smooth and textured implants can usually be differentiated. The smooth wall device is seen to be more sharply demarcated from the underlying anechoic gel. The textured device appears to be fuzzier in appearance and thicker than its smooth counterpart. Breast implants, despite being placed properly into the surgically created pocket in an upright position, can spontaneously flip upside down such that the posterior patch now lies in the more anterior position and can be visualized easily by HRUS. On ultrasound, the upside-down breast implant image shows an overlap of a double echogenic line representing the elastomer shell overlying a slightly thicker, single echogenic line representing the posterior patch. The consistent distance of the overlap is symmetric with the opposite side of the patch. This symmetry of overlap and single line echogenic structure of the patch separates this otherwise normal implant from the "subcapsular line" of the broken silicone gel breast implant (Fig. 13.6).

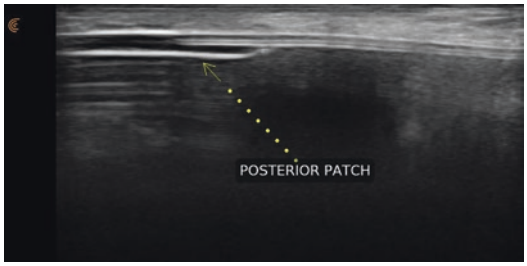

Fig. 13.6 Grayscale ultrasound image of the posterior patch of a silicone gel breast implant

13.5 Saline and Structured Saline Breast Implants

Saline breast implants are made from the same elastomer shell as silicone breast implants. Rather than being filled with a silicone gel, these implants are filled with sterile saline. Saline implants contain a filling valve on the anterior surface of the implant, which is readily identifiable by ultrasound. The valve appears as a discontinuous outer shell with a saucer-shaped echogenic line just below the anterior surface of the shell. A new type of saline breast implant is referred to as being a "structured saline implant." These implants contain more than one saline filled chamber and each chamber has its own filling port. One port is on the anterior surface of the shell and the other on the posterior (Fig. 13.7).

The structured saline breast implant has a distinctive ultrasound appearance of an implant within an implant. The peripheral edge of a saline implant will differ in ultrasound appearance from that of a silicone gel filled elastomer. Because of the slowing ultrasound waves as they travel through silicone gel compared to saline, the soft tissues seen posterior to the silicone gel implant seem to appear to be further away creating a "step off phenomena." Broken saline breast implants do not represent the diagnostic challenge of a broken silicone gel breast implant. Most commonly, saline implant failures become self-evident in a matter of day as the saline within the lumen of the implant escapes the confines of the elastomer as the implant collapses from volume loss. On ultrasound, the broken saline breast implant is seen as a series of superimposed echogenic lines with a variable amount of anechoic

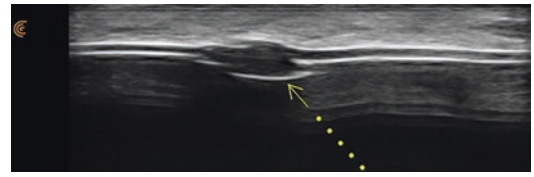

Fig. 13.7 Grayscale ultrasound image of smooth saline filled breast implant. Arrow shows the filling valve on the anterior surface of the implant

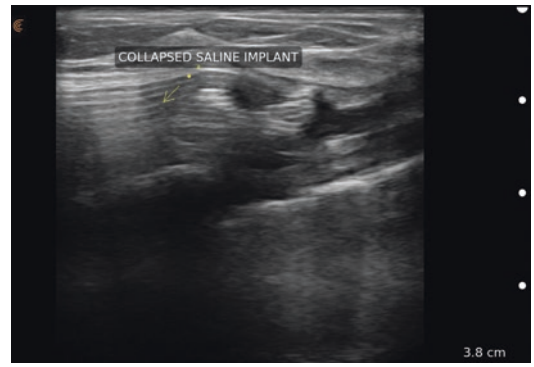

Fig. 13.8 Grayscale ultrasound image showing a saline breast implant that has collapsed with loss of most of its saline volume

space between representing retained saline within the elastomer. HRUS can be helpful in intraoperative localization of the collapsed broken saline implant (Fig. 13.8).

The periprosthetic breast capsule can retract to accommodate the decreased volume of the broken saline breast implant. This can make it difficult for the plastic surgeon to locate the implant through an infra-mammary crease approach as the broken saline implant migrates upward towards the axilla. Using HRUS during the procedure, the plastic surgeon can better adjust the plane of dissection to more easily locate the broken implant.

13.6 Ultrasound Imaging of Broken Silicone Gel Breast Implants

The incidence of silicone breast implant rupture is presently unknown. Older silicone gel breast implants with thin elastomeric shells and honey-

like gel viscosity are known to have rupture rates of 50% at 12 years or more since implantation [25]. Rupture rates with newer 5th generation silicone gel breast implants have improved to 10–14% at 8–10 years post implantation [26]. Breast implant rupture can be contained within the fibrous capsule surrounding the implant and is called intracapsular rupture. Should the implant filler silicone gel migrate beyond the confines of the fibrous capsule, this is termed extracapsular rupture. Seventy-seven to eighty nine percentage of silicone gel breast implant ruptures are intracapsular and are usually asymptomatic [15]. In older, thin elastomer shell implants filled with a less cohesive gel, one of the ultrasound signs of implant failure is the "stepladder sign" [13, 24, 27–34]. The stepladder sign on HRUS appears as a series of multiple, discontinuous linear echoes representing the folding of the elastomer shell into the inside of the silicone gel of the implant (Fig. 13.9).

This corresponds to the "linguine sign" seen on MRI. As silicone gel extravasates beyond the confines of the elastomer shell, it may come into contact with fluid surrounding the implant. The ensuing phase aberration of the ultrasound beam causes the silicone gel to take on a "snowstorm" appearance [28, 35] (Fig. 13.10).

This snowstorm appearing gel can be seen in both intracapsular implant failure as well as silicone blebs seen outside of the fibrous capsule and silicone filled lymph nodes seen along the lateral border of the pectoralis major and in the axilla. Another commonly seen sign of intracapsular rupture is the "noose" or "keyhole" [36, 37] (Fig. 13.11).

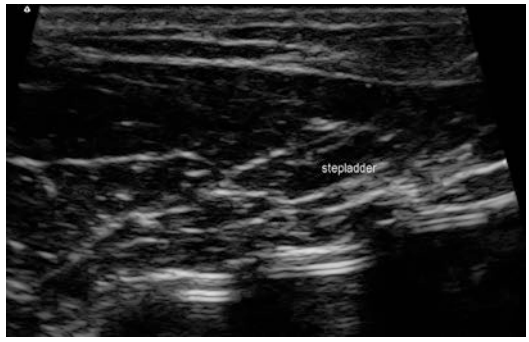

Fig. 13.9 Grayscale ultrasound image of broken silicone gel breast implant exhibiting the stepladder sign

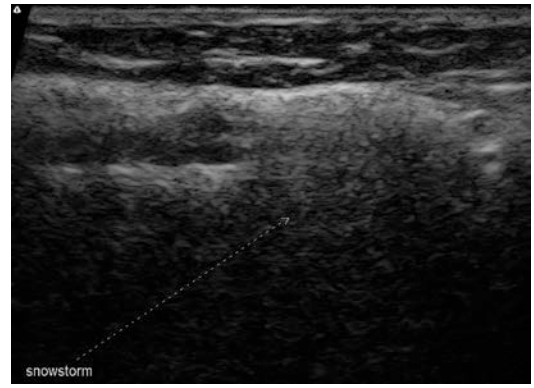

Fig. 13.10 Grayscale ultrasound image of broken silicone gel breast implant exhibiting the snowstorm sign

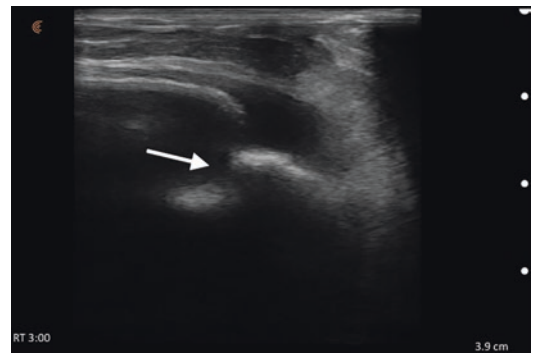

Fig. 13.11 Grayscale ultrasound image of broken silicone gel breast implant exhibiting the keyhole sign. Arrow depicts the midportion of the keyhole

Seen more often in older, less cohesive silicone gel implants, the in-folding of the implant elastomer shell produces a fold which can allow the internal silicone gel to escape through small disruptions of the elastomer shell and occupy the apex of the fold. One of the advantages of using HRUS in the evaluation of possible silicone gel breast implant failure in comparison to MRI is the dynamic nature of the HRUS exam. Using HRUS, the sonographer has the ability to change the configuration of the shell of the implant by the placement of extrinsic pressure on the implant. The finding of a deep fold in an implant may look like a "Noose or Keyhole sign" until extrinsic pressure is applied opposite the fold. As the shell distends and unfolds, the sonographer

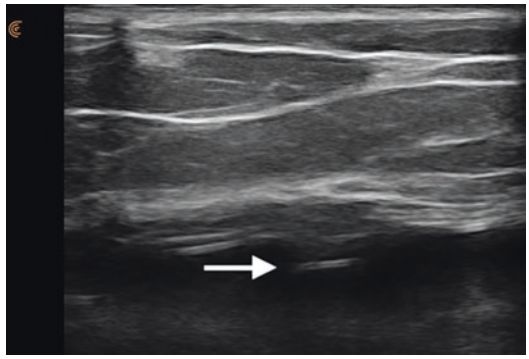

Fig. 13.12 Grayscale ultrasound image of broken silicone gel breast implant exhibiting the subcapsular sign. Arrow depicts the fragment of elastomer

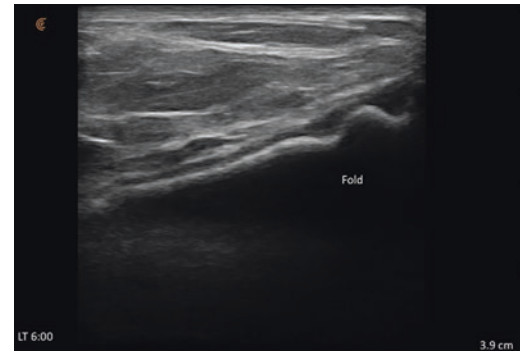

Fig. 13.13 Grayscale ultrasound image of a silicone gel breast implant exhibiting the wavy folds of the elastomer shell

may be able to visualize a filling out of the fold. The actual continuity of the shell would suggest that this is merely a fold and the implant is actually intact. The elastomer shell may fragment with pieces of the shell appearing within the internal silicone gel as a linear echogenic line. This linear echo is referred to as the "subcapsular line" [29, 38–41] (Fig. 13.12).

In the situation where there is complete or near complete collapse of the elastomer shell, the segment of shell embedded into the depths of the remaining silicone gel may be deeper than can be visualized with high-frequency transducers. It may be necessary to image the deeper aspect of the silicone gel breast implant with lower frequencies [42].

13.7 Mimic Signs of Intracapsular Rupture

There are several ultrasound findings that may confound the diagnosis of a ruptured silicone gel breast implant. One of the more common findings seen in an intact silicone gel implant is a fold (Fig. 13.13).

Until the most recent iteration of cohesive silicone gel implants, most implants were not filled to the maximum capacity of the silicone elastomer shell. This would allow for some collapse of the implant shell along the periphery of the implant. Normal folds can have either an anechoic or mildly echoic fluid between the implant shell

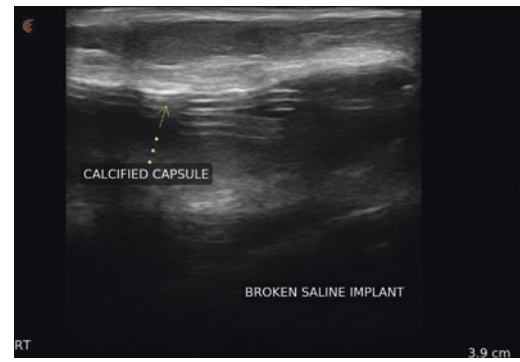

Fig. 13.14 Grayscale ultrasound image of broken saline breast implant with a hyperechoic appearance of the implant capsule suggesting calcification of the capsule

and the fibrous capsule. In the presence of capsular contracture, where the breast periprosthetic fibrous capsule becomes tight and nondistensible, numerous folds may be visualized. In the situation of a tight capsular contracture, an infolding of the breast implant may be so deep that the ultrasound appearance may appear to be a "keyhole" or "noose" sign giving a false positive ultrasound reading of a broken silicone gel implant. Long standing silicone gel implant capsules may become calcified. This will present as areas of higher echogenicity within the fibrous capsule. Scattered, fine calcifications may not obscure visualization of the breast implant elastomer. More dense, confluent calcifications may cause acoustic shadowing and obscure the normal trilaminar appearance of the shell–capsule interface making diagnosis of rupture difficult (Fig. 13.14).

Over time, newer, highly cohesive silicone gel implants may develop changes to the structure of the internal gel while maintaining the integrity of the elastomer shell. Gel fractures or gel bubbles may occur within the internal gel of the implant (Fig. 13.15). The normal anechoic internal gel of the implant may contain echogenic areas within the implant fill material. The ultrasound images of these cohesive gel changes within the internal confines of the implant may mimic the "stepladder" or "subcapsular line" seen with broken silicone gel implants. These internal echoes with an overlying intact shell are poor predictors of the loss of shell integrity. Gel bubbles can also mimic the appearance of a broken silicone gel breast implant. The differentiating clue is the consistent width of a reverberation-type artifact appearance seen just below an intact overlying elastomer shell (Fig. 13.16). Seen in an ex vivo implant, the reverberations take on a cylindrical appearance matching the dimensions of the bubble (Figs. 13.15 and 13.16).

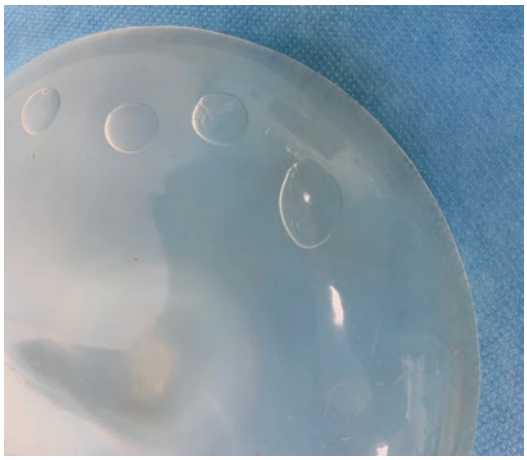

Fig. 13.15 Silicone gel breast implant with bubbles within the internal gel. The elastomer shell is intact

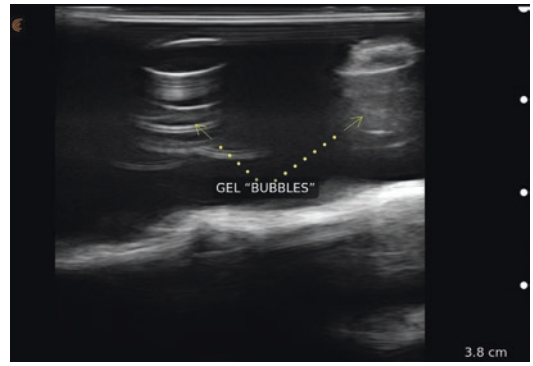

Fig. 13.16 Grayscale ultrasound image of an ex vivo silicone gel breast implant exhibiting echogenic swirling lines indicative of gel bubbles

13.8 Shaped Breast Implant Rotation

Silicone and saline breast implants can be manufactured in both round and anatomically shaped configurations. The Allergan 410 (silicone gel) and 468 (saline) have orientation "knobs" of an additional thicker silicone elastomer strategically placed on the anterior surface of the implant to aid the plastic surgeon in vertical alignment of the implant in the pocket (Fig. 13.17).

These orientation "knobs" can be visualized with HRUS on the anterior surface of the implant. Although the implant may have been orientated vertically during its initial insertion, these implants may rotate causing a distortion of the look of the augmented breast. HRUS may be used to locate the orientation "knobs." By transposing the location of both of the orientation "knobs" found on HRUS to the skin, an assessment of the rotation of the implant from vertically can be determined.

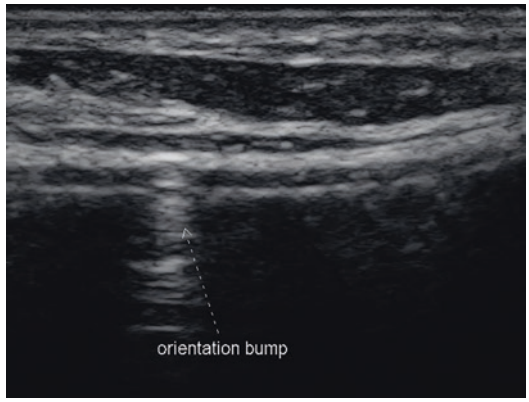

Fig. 13.17 Grayscale ultrasound image of a shaped Allergan 410 silicone gel breast showing the orientation bump on the surface of the elastomer. Posterior acoustic shadowing is seen below the echogenic line indicating the location of the palpable bump

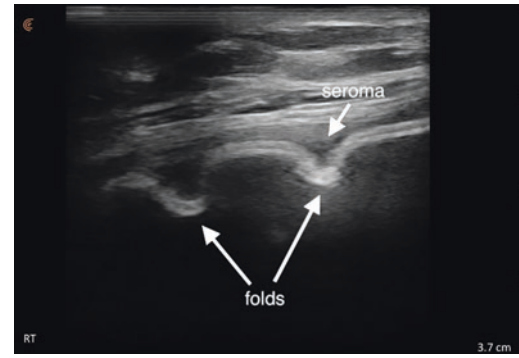

Fig. 13.18 Grayscale ultrasound image of a breast implant exhibiting capsular contracture. Multiple folds and a small amount of seroma are seen

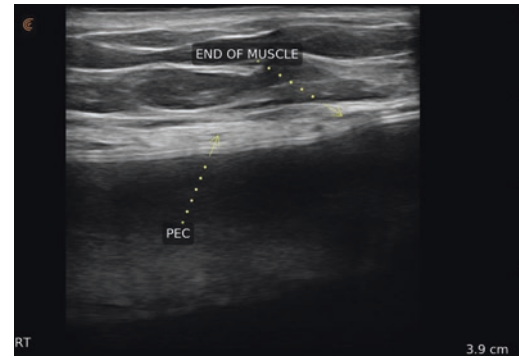

Fig. 13.19 Grayscale ultrasound image of a breast implant imaged at the medial border of the implant at the level of the mid portion of the areola. The transition of the implant from the submuscular to the subglandular position is demonstrated

13.9 Capsular Contracture

One of the known common adverse outcomes of the placement of breast implants is the formation of an unyielding fibrous capsule surrounding the breast implant called capsular contracture [42, 43] (Fig. 13.18).

The Baker classification is used to describe fibrous breast implant capsules [44]. Grade 1 capsules allow for a normal feeling and appearing breast. Grade 2 capsules feel more firm than normal. Grade 3 capsules feel firmer and make for a visible distortion of breast shape. A Grade 4 capsule has the characteristics of a Grade 3 capsule and adds the fact that the patient experiences pain as well. The most commonly seen finding on HRUS for a breast implant with capsular contracture is folds. There may be a series of multiple folds or a single deep fold. HRUS is used by plastic surgeons in the evaluation of capsular contracture. Capsular contracture does not usually appear for many months to years after breast implant placement. Patients will sometimes be seen and complain of a breast implant that remained high on the chest wall and never dropped into the more desired position where the middle of the implant corresponded to the overlying nipple. In submuscular implant placement, the post-surgical subsequent tightening of the pectoralis major muscle will disallow gravitational descent of the breast implant. HRUS can be used to evaluate early capsular contracture and distinguish inherent thickening and lack of distensibility of the capsule (true capsular contracture) from incomplete division of the rib origins of the pectoralis major muscle which leave muscle fibers below the mid portion of the implant thereby holding it higher on the chest wall than its more inferior desired position. By scanning the medial aspect of the breast implant capsule at the level of the areola, the point of transition of the submuscular and subglandular position of the breast implant can be visualized and compared to the side with the correct implant position (Fig. 13.19).

Based on the visualization of the level of muscle division being different on the affected side, the plastic surgeon may decide to divide some of the muscle origins of the pectoralis muscle as well as the capsule in an attempt to lower the involved implant.

13.10 Seroma and Hematoma

Small fluid collections surrounding breast implants can occur in the absence of any pathology. Anechoic or slightly diffuse hyperechoic fluid collections can be visualized between the capsule surrounding the implant and the elastomer shell. These small seromas may be seen relatively soon after implantation of implants or any surgical manipulation of the breast implant capsule such as a capsulotomy, capsulectomy, or capsulorraphies. Late seroma, 1 year or more after breast implant placement occur in 0.1–0.2% of textured silicone gel breast implants [45] (Fig. 13.20).

Etiology of breast implant seroma can be post traumatic, post-surgical, infectious, idiopathic, or rarely due to breast implant-associated (BIA) anaplastic large cell lymphoma (ALCL). BIA-ALCL is a rare T cell lymphoma that presents a delayed periprosthetic fluid collection (60–90%) or a capsular mass (40%) at an average of 8–10 years after textured breast implant placement [46]. The cases are almost evenly split between post reconstructive and cosmetic placement of textured breast implants. Late breast implant seromas will require evacuation. Ultrasound is useful to allow visualization of the breast implant during breast seroma aspiration. The patient is placed in the supine position on the bed with the head slightly elevated to allow gravitational descent of the fluid. The breast implant is pushed upward and away from the site of needle penetration, usually at the inframammary crease. Various types of needles such as the Veress® needle [47], Sonosite® needle, and blunt cannulas such as the Seromacath® [48] have been described as being useful and safe for periprosthetic fluid aspiration. A linear high-frequency probe (9–14 MHz) is used (Fig. 13.21).

The ultrasound transducer is placed on the skin of the breast overlying the needle and oriented as parallel to the plane of the needle as possible. This is termed the "in-plane technique." Some HRUS devices have a software enhancement of the underlying needle making it easier to visualize. As the plane of the transducer moves away from parallel to the plane of the needle, only portions of the needle may be visualized. Because of the importance of visualization of the tip of the needle in order to best avoid penetration of the implant shell, enhancements of the external geometry of needles such as the Sonosite® allow reflection of the ultrasound waves at sharper angles such that needle visualization is improved at steep beam

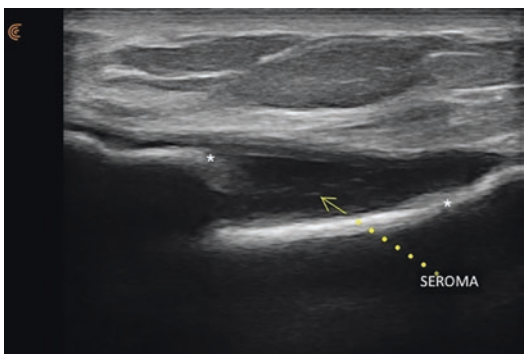

Fig. 13.20 Grayscale ultrasound image of a broken silicone gel breast implant with mostly anechoic fluid between the elastomer shell and the periprosthetic capsule. * denotes the elastomer shell

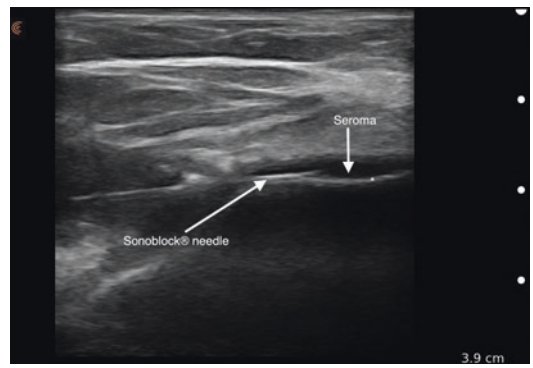

Fig. 13.21 Grayscale ultrasound image of a breast implant seroma being aspirated with a needle. * denotes the elastomer shell of the breast implant

angles. Examination of the fluid aspirate includes culture and sensitivity for infectious etiology and CD30 immunohistochemistry for the diagnosis of BIA-ALCL. At least 50 mL of fluid is necessary for CD30 testing. Ultrasound may be useful in the evaluation of the swollen breast in the immediate postoperative time period. In mastopexy with breast implant placement, there are two potential cavities in which blood or fluid may collect. Early hematoma after mastopexy with implants can appear in the subcutaneous tissue surrounding the areola or within the newly established pocket created for the breast implant. Ultrasound is useful in separating the diffuse echogenic soft tissue appearance of edema from an actual collection of fluid. Seromas will appear anechoic on ultrasound, while a hematoma may have areas of echogenicity within a mostly anechoic space. New hematomas may be difficult to evacuate through a small-bore cannula or needle because of the semi-solid nature of the blood. After clot retraction takes place naturally over a 7–10-day period of time, the ultrasound image becomes less echogenic and takes on the look of an anechoic seroma. At this point in time, the more liquid consistency of the seroma makes HRUS guided aspiration easier.

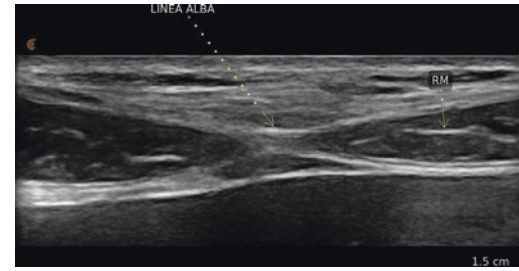

Fig. 13.22 Grayscale ultrasound image of the normal appearance of the abdominal midline with transducer oriented transversely just above the umbilicus. RM is rectus abdominis muscle

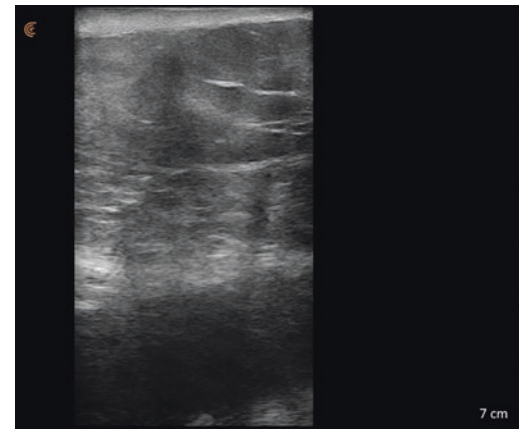

Fig. 13.23 Grayscale ultrasound image of edema of the abdominal wall. Diffuse hyperechoic shadows obscure the normal hypoechoic soft tissue

13.11 Abdomen

The typical ultrasound appearance of the unoperated abdomen, with the transducer in the transverse orientation over the midline replicates the appearance of a "bowtie." The confluence of the anterior rectus fascia from each side form the linea alba of the rectus abdominis as its center and the sides of the "bowtie" represent the splitting of the anterior and posterior fascias as they separate to include the rectus abdominis muscle within (Fig. 13.22).

HRUS evaluation of anterior abdomen in the plastic surgical patient considering abdominoplasty or suction-assisted lipectomy of anterior abdominal wall may be a useful adjunct to physical exam in detecting unrecognized ventral hernias. Where separation of the midline fascia is seen, a Valsalva maneuver may reveal escape of preperitoneal fat or actual peritoneal contents such as small bowel through the fascial opening. HRUS has demonstrated to be useful in the evaluation of the postoperative body contouring patient. When patients present with a contour deformity after plastic surgery of the trunk, the question that needs to be addressed is whether this represents edema or a collection of blood or serum. The ultrasound image of edema is easily recognized as a diffuse, homogeneous increase in echogenicity throughout the entire image (Fig. 13.23)

In contrast to the image of edema, the HRUS image of a seroma is that of a well-demarcated anechoic area within the surgical area and corresponds to the visual location of the contour deformity (Fig. 13.24).

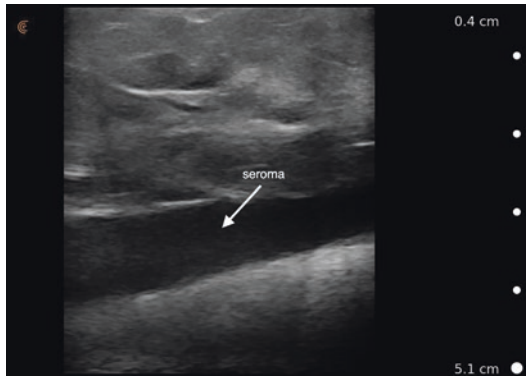

Fig. 13.24 Grayscale ultrasound image of a seroma of the anterior abdominal wall

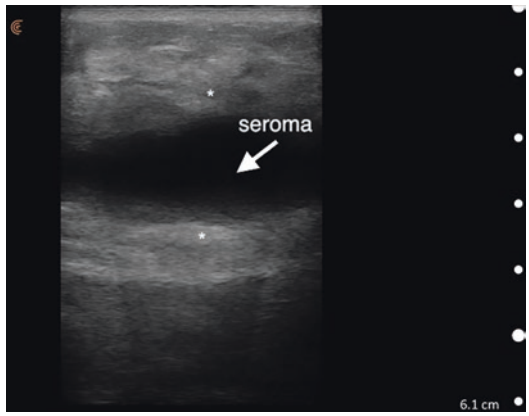

Fig. 13.25 Grayscale ultrasound image of a pseudo-bursae of the anterior abdominal wall. * denotes the hyperechoic hyalinized thickened tissue surrounding the fluid

Abdominal seromas can be easily aspirated under HRUS guidance. Using sterile technique, an ultrasound enhancing needle such as the Sonosite® can be inserted using an "in-plane" technique to aspirate the seroma. Post aspiration ultrasound can confirm the removal of the seroma and follow-up ultrasounds can be done to confirm that the seroma does not reoccur. Recurrent seromas, despite successful serial aspirations, may allow for a thickened scar capsule to surround the seroma cavity. The internal lining becomes hyalinized and continues to produce fluid. These persistent seromas are called pseudo-bursae. HRUS imaging of a mature pseudo-bursae shows an echogenic capsule surrounding an anechoic center (Fig. 13.25).

Minimally invasive techniques such as injections of a sclerosant solution into the pseudo-burse have been described. Should these minimally invasive procedures not be successful in eliminating the pseudo-bursae, a surgical approach may become necessary. Complete excision of the pseudo-bursae with subsequent elimination of the dead space between the abdominal fascia and the overlying fat is usually curative in restoring the normal contours of the trunk.

HRUS has shown to be helpful in marking the patient prior to high-definition liposuction. In high-definition liposuction, the goal is to accentuate the visualization of the underlying musculature of the abdomen, chest, or extremities. The muscle interfaces such as the plica semilunaris, where the external abdominal oblique muscle attaches to the lateral aspect of the rectus abdominis can be visualized with HRUS. The rectus abdominis has transverse thickened areas of fascia that correspond to the location of vascular perforators. These inscriptions can be visualized with HRUS and marked in the overlying skin to indicate an area where more fat will be removed. While transition zones between muscles can then be accentuated with more superficial fat removal, the addition of fat into the muscle can accentuate its visibility through the skin. HRUS can be used during the fat grafting procedure to visualize the direct transfer of the fat graft to the intramuscular position.

13.12 Nerve Blocks

Regional nerve blocks, once only performed by anesthesia providers, can also be administered to plastic surgery patients by the plastic surgeon using HRUS. The 2 most commonly done HRUS-guided nerve blocks done by plastic surgeons are the pectoralis nerve block (PECS block) and the transversus abdominis plane block (TAP block). The placement of breast tissue expanders for post mastectomy breast reconstruction and breast implants for cosmetic enhancement of the breast both can be done with placement of the prosthesis under the pectoralis muscle.

The post procedure spasm of the pectoralis major muscle can lead to a painful experience for the patient and can delay the descent of the breast prosthesis into the more desired, inferior aspect of the submuscular pocket. The pectoralis major and minor muscles are innervated by the medial and lateral pectoral nerves. The lateral pectoral nerve originates from the lateral cord of the brachial plexus (C5, C6, C7). It penetrates the clavipectoral fascia to directly innervate the pectoralis major muscle. The medial pectoral nerve originates from the medial cord of the brachial plexus (C8, T1). It penetrates the deep surface of the pectoralis minor muscle, traverses this muscle, and innervates the pectoralis major muscle from its deep surface. The original PECS block was first described by Blanco [49]. He described a cranial to caudal approach over the clavicle with a linear probe. Using a high-resolution linear probe, the thoraco-acromial artery was located with color Doppler in the fascial plane between the pectoralis major and minor muscles. The lateral pectoral nerve travels in the fascial plane between the pectoralis major and minor muscles along with the thoraco-acromial artery. A 50 mm ultrasound block needle was inserted with an "in-plane" technique through the pectoralis muscle and into the fascial plane between the pectoralis major and minor muscles. Levobupivacaine 0.25% was injected at a volume of 0.4 mL/kg. Perez described an alternative approach at the lateral third of the clavicle with the transducer aligned perpendicular to the axis of the body and passing the needle from medial to lateral after locating the thoraco-acromial artery [50]. The author has described another approach called the lateral approach pectoralis block (LAP). In this method, the ultrasound needle is passed in plane from under the lateral border of the pectoralis major muscle toward the previously located thoraco-acromial artery in a lateral to medial direction. After needle visualization in the fascial plane between the pectoralis major and minor muscles, a test dose of normal saline will confirm the correct location with an anechoic space that separates the two muscles (Fig. 13.26)

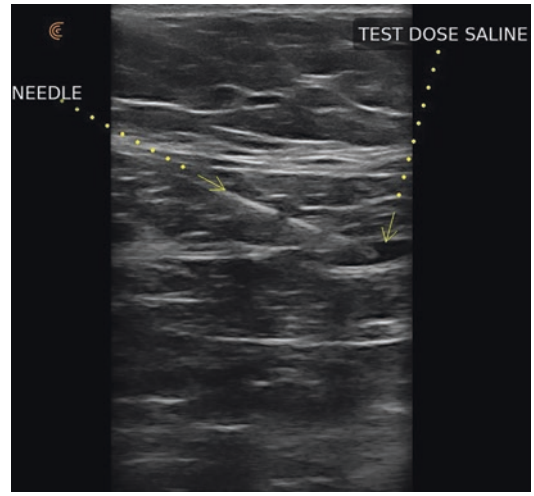

Fig. 13.26 Grayscale ultrasound image of chest wall showing Sonoblock® needle in the space between pectoralis major and minor muscles. A test dose of saline is injected producing an anechoic space between the muscles

The local anesthetic is then deposited in the plane between the pectoralis major and minor muscles along the entire path of the needle from the lateral border of the pectoralis major to the location of the lateral pectoral nerve. This approach has several advantages. It can be done from the side of the bed while the anesthesia provider is attending to tasks at the head. The path of the needle deposits the local anesthetic over the perforating branches of the medial pectoral nerve as they pierce the undersurface of the pectoralis major for an improved block of the inferior aspect of the pectoralis major muscle (Fig. 13.27).

The original PECS block can be augmented with a second injection (PECS 2) placed between the pectoralis minor and serratus anterior muscles. The PECS 2 block adds anesthesia to the lateral chest wall and axilla by blocking intercostal nerves 3–6, intercostobrachial and long thoracic nerves. The PECS blocks have been shown to be effective in lowering visual analog pain scores as well as opiate requirements after breast surgeries [51–53].

HRUS can also be used to provide anesthesia to plastic surgery procedures performed on the anterior abdominal wall. This block can be useful

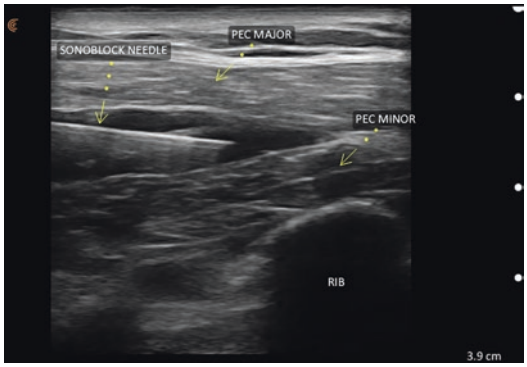

Fig. 13.27 Grayscale ultrasound image of chest wall showing an increased size of the anechoic space separating the pectoralis major and minor muscles

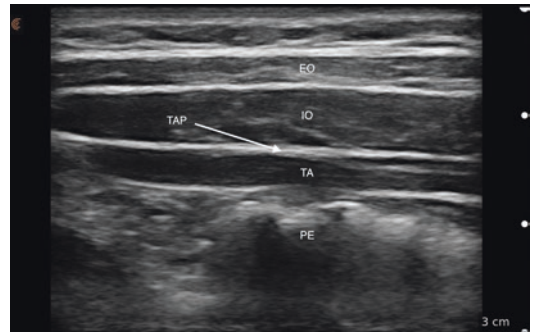

Fig. 13.28 Grayscale ultrasound image of abdominal wall. Transverse view above umbilicus at the anterior axillary line. *EO* external abdominal oblique muscle, *IO* internal abdominal oblique muscle, *TA* transversus abdominis muscle, *TAP* transversus abdominis plane, *PE* peritoneum

for abdominal wall reconstruction, transverse rectus abdominis muscle (TRAM) or deep inferior epigastric flaps (DIEP) and abdominoplasties. Sensory innervation of the anterior abdominal wall is from the anterior branches of the intercostal nerves T 7-12 and the anterior rami of the first lumbar spinal nerve which travel in the plane between the transversus abdominis muscle (TA) and the internal oblique muscle (IO). The transversus abdominal plane (TAP) block was first described by Hebbard [54] (Fig. 13.28).

There are three distinct locations where the (TAP) block can be administered. The Lumbar approach injects at the triangle of Petit. The lateral approach is done in the mid abdomen and the oblique subcostal approach between the posterior rectus sheath and the (TA). The lateral mid abdominal TAP block is typically done with the patient in the supine position after the induction of anesthesia. A high-resolution linear probe (7–14 MHz) is positioned at the anterior to mid axillary line, halfway between the subcostal region and the iliac crest. Depth is adjusted such that the TAP plane is visible in the midfield of the image. External abdominal oblique (EO) muscle can readily be seen below the subcutaneous fat layer. The 3 muscles of the abdominal wall, (EO), (IO), and transversus abdominis (TA) can be visualized from superficial to deep with the (IO) usually being the most prominent in thickness. Below the (TA) is the preperitoneal fat and the contents of the peritoneum. Small bowel peristalsis is often visible. If difficulty in finding all three muscles is encountered, the probe can be moved more medially over the rectus abdominis muscle (RA). Tracing out laterally toward the mid axillary line, the (RA) will be seen to taper and a single echogenic fascia, the plica semilunaris, will become evident. Moving the probe toward the anterior axillary line, the 3 distinct muscle layers will become apparent. A 100 mm, 20-gauge to 22-gauge Touhy tip, sonographic needle (Sonosite® or Braun®) is introduced from medial to lateral. As the TAP is entered, there is usually the feeling of a "pop," and a rebound of the (TAP) in an upward direction is seen on the ultrasound image. In order to confirm the needle tip location within the (TAP), a small 1–2 cc dose of normal saline can be given. A hydro-dissection of the (TAP) is seen as a confluent anechoic separation of the (IO) and the (TA). Should the needle tip not be properly positioned within the (TAP), injection into either the (IO) or the (TA) will produce a diffuse echogenic cloudy appearance within the muscle. Should intramuscular injection proceed proper location of the (TAP), it is prudent to pull the needle back toward the (IO) and try to enter the (TAP) in a new location where the anechoic spread can be more easily identified. The use of local anesthetics in a TAP block, such as liposomal bupivacaine (Exparel®, Pacira

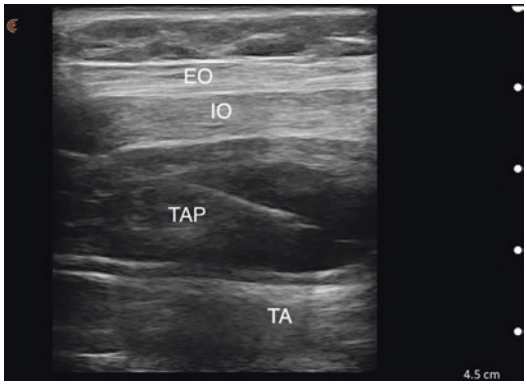

Fig. 13.29 Grayscale ultrasound image of abdominal wall. Transverse view above umbilicus at the anterior axillary line. *EO* external abdominal oblique muscle, *IO* internal abdominal oblique muscle, *TA* transversus abdominis muscle, *TAP* transversus abdominis plane. Anechoic spread of local anesthetic in TAP

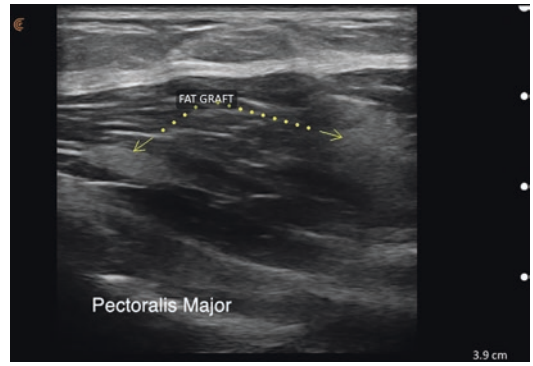

Fig. 13.30 Grayscale ultrasound image of chest wall. Hyperechoic parcels of fat are seen the normal striations of the pectoralis major muscle

Pharmaceuticals, San Diego, Ca) with 72 h durations of effect, has been shown to be effective in pain relief and a decrease in the use of opiates for patients undergoing surgery of the anterior abdominal wall [55–57] (Fig. 13.29).

13.13 Ultrasound Use in Fat Grafting

Autologous fat grafting was first described by Gustav Neuber in 1893 [58]. He grafted fat from the arm to the inferior orbital rim for a depressed scar caused by osteomyelitis. Plastic surgeons today use fat grafting in both reconstructive and cosmetic procedures. Fat is harvested with liposuction cannulas under lower negative pressures to preserve the integrity of the adipocytes. The fat is usually processed by filtration, centrifugation, or gravity-based decantation to remove the cell fragments, blood, and fluid. Fat survival is better with intramuscular injections where vascularity is more robust than the subcutaneous fat layer. Intramuscular fat injections are used by plastic surgeons for cosmetic enhancement of muscles such as the pectoralis, deltoid, and abdomen (Fig. 13.30).

In high-definition liposuction, the deep fat below the superficial fascia is removed and superficial sub dermal fat is removed over natural muscle depressions. Fat grafting can then be used under ultrasound guidance to ensure proper placement of fat within the muscle and avoid penetration of the fat grafting cannula into undesirable locations such as the chest wall, peritoneal cavity, or breast implant. The "in plane" technique is used with a linear high-frequency probe under sterile conditions. Newer wireless ultrasound devices such as the Clarius L7 and L15, (Clarius, Vancouver, BC) have made the intraoperative, sterile, application of ultrasound easier than having an ultrasound transducer covered by a sterile condom to a fixed length cord draped over the sterile field. The wireless devices have the advantage of transmitting the ultrasound image to a wide variety of both Android and IOS devices, which can be more easily moved during the procedure allowing comfortable viewing angles by the operating plastic surgeon. The ultrasound-guided fat grafting procedures are usually begun by first identifying the muscle target. Depth of the ultrasound beam can be adjusted such that the needle penetration is in the mid field of the image. Color Doppler imaging of the surrounding vasculature will help make entry points for the fat grafting cannula in safe locations to avoid vascular injury. The fat grafting procedure can be done in real time by first introducing the cannula into the muscle under ultrasound visualization. The fat can then be injected as the cannula is withdrawn. Post injection visualization of

the injected fat will confirm proper location of the fat graft and allow the plastic surgeon to discern what areas of the desired fat graft location still have not been grafted. This will allow for a more even distribution of the fat graft and improve fat graft viability. Fat grafting may also be done in a subcutaneous plane. For breast reconstruction patients, fat may be added to improve symmetry and add volume to the breast. Liposuction soft tissue defects can also be improved by fat grafting into the subcutaneous plane. Ultrasound can be used to measure the size of the defect and monitor the progression of fat taken to the recipient site.

According to the American Society of Plastic Surgeons Procedural Statistics, gluteal fat grafting or the so-called Brazilian buttock lift (BBL) was the fastest growing cosmetic procedure in 2018 with a 19% increase over 2017 and 256% increase since 2000 [1]. However, there has been an alarming number of deaths reported associated with this procedure [59–61]. All of the fatalities have been attributed to fat embolism. It is postulated that the injected fat gains access to the gluteal veins either by direct injection or by injury to the vessel allowing the fat nearby to migrate into the vessel due to the negative pressure of the large gluteal vein [61]. In 2018, the American Society of Plastic Surgeons produced a Gluteal Fat Grafting Advisory stating that gluteal fat grafting should only be done in the subcutaneous space [62]. The use of ultrasound in real time to visualize the location of fat graft deposition into the subcutaneous space of the gluteal region has been described [63]. A linear transducer with a frequency range of 7-12 MHz will allow for good visualization of the buttock in the vast majority of patients. Lower frequency probes will allow for better visualization at deeper locations but will have less resolution. Depth is adjusted such that the gluteal muscle and fascia are visualized. The superficial gluteal fascia is identified as an echogenic line separating the superficial and deep fat compartments of the buttock (Fig. 13.31).

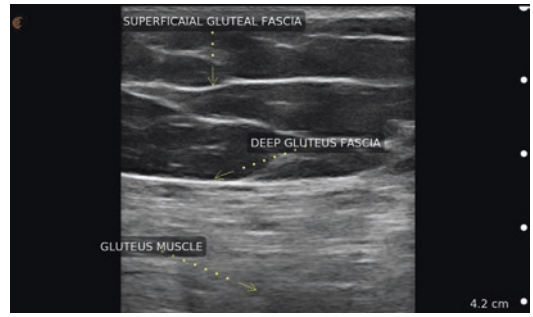

Fig. 13.31 Grayscale ultrasound image of gluteal region. Normal anatomy of buttock showing the subcutaneous space separated by the echogenic superficial gluteal fascia. The deeper echogenic line represents the deep gluteal fascia overlying the gluteal muscle

Vertically oriented fibrous septae can be seen emanating from the superficial gluteal fascia and attaching to the deep surface of the overlying dermis. Doppler ultrasound is used to locate and mark on the skin surface the location of the superior and inferior gluteal arteries. The fat is harvested with a variety of different liposuction techniques and processed with various filtration methods. Using stiff fat grafting cannulas, from access sites that will allow for cannula location to remain superficial to the deep gluteal fascia, the fat is injected under visualization of ultrasound. It is preferable to begin the fat deposition in the plane between the deep and superficial gluteal fascias. Ultrasound image of fat in the subcutaneous space appears as a diffuse echogenic infiltrate that obscures the normal mostly hypoechoic subcutaneous space (Fig. 13.32).

Post fat injection imaging will allow the plastic surgeon to visualize areas that are either incompletely filled or have not had fat injected allowing the surgeon to produce a more homogenous result. Subcutaneous only placement of fat grafts during a BBL is thought to be protective of inadvertent fat injection into the gluteal muscles and will therefore allow for safe placement of fat grafts without the risk of fat embolism [51].

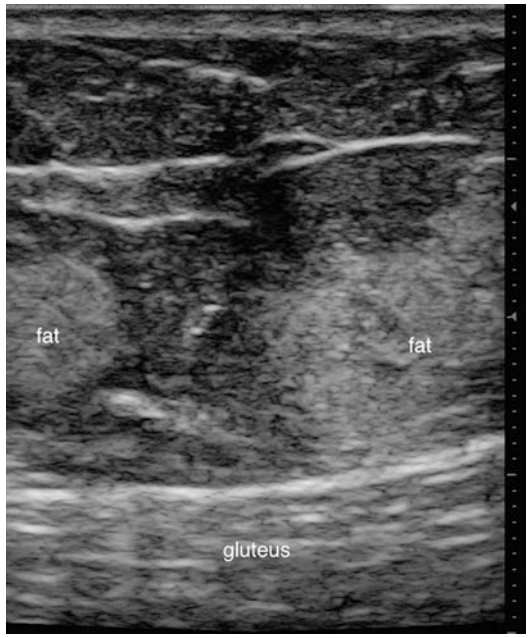

Fig. 13.32 Grayscale ultrasound image of gluteal region. Hyperechoic deposits of fat grafts obscure the normal hypoechoic fat of the buttock region

13.14 Fillers

Dermal fillers are the second most common non-invasive cosmetic procedure (after Botulinum toxins) done by plastic surgeons in the US. According to the American Society of Plastic Surgeons Procedural Statistics for 2018, 2,676,970 soft tissue fillers were done by Board Certified Plastic Surgeons [1]. Soft tissue fillers are used primarily in the face to enhance volume loss, fill in subcutaneous defects, smooth out wrinkles and folds, and improve the appearance of surgical and acne scars. Soft tissue fillers can be separated into two broad categories: biologic fillers and synthetic fillers. Biologic fillers, such as hyaluronic acids (HA), are resorbable sugars and are the most commonly used filler. Permanent fillers such as calcium hydroxyapatite (CaHA) and polymethyl methacrylate (PMMA) are also used to add volume to the dermis and subcutaneous tissues. Hyaluronic acid is a high-molecular-weight polysaccharide which binds water. HA can be either of avian source or made from synthetic fermentation from bacteria. The variables in the formulations of the currently available HAs are particle size, concentration, and the amount of cross-linking. Larger particle size and more cross-linking in the HA formulation will lead to more duration of effect. Higher concentrations of HA will osmotically bind more water and have a more profound effect on increasing the apparent volume correction from the filler. The immediate appearance of HA after injection into the soft tissues using HRUS is that of mostly anechoic spaces of ovoid shape that may contain some internal debris echoes (Fig. 13.33).

As the HA becomes more integrated into the surrounding soft tissues, the HRUS image of the filler becomes more difficult to discern from normal tissue. Calcium hydroxyapatite, Radiesse® (Merz, Raleigh, NC), is a suspension of microspheres of calcium hydroxyapatite crystals in an aqueous gel carrier consisting of sterile water, glycerine, and sodium carboxymethylcellulose. Radiesse® is considered a biostimulator as it causes neocollagenesis in response to the injected calcium hydroxyapatite crystals. On HRUS, Radiesse® appears as multiple hyperechoic deposits with variable degrees of posterior acoustic shadowing (Fig. 13.34).

Polymethylmethacrylate, BellaFill®, is PMMA microspheres in a bovine collagen matrix with 0.3% lidocaine. It is considered a permanent filler with duration of effect lasting 5 years or more. It is mostly used as an intradermal filler for the naso-labial folds, acne scars, and soft tissue defects. Early, less than 3 months after PMMA injection, HRUS images reveal multiple

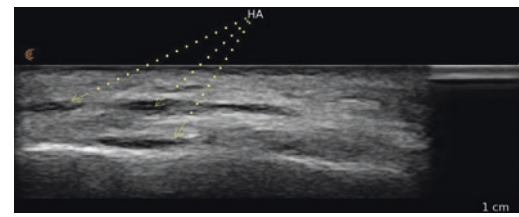

Fig. 13.33 Grayscale ultrasound image of cheek immediately after injection of hyaluronic acid filler. Anechoic deposits of the filler are seen within the fat of the cheek

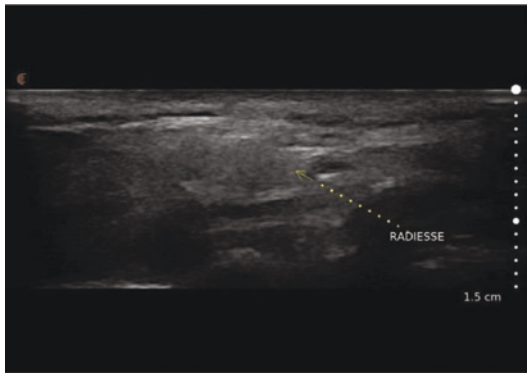

Fig. 13.34 Grayscale ultrasound image of the cheek after calcium hydroxyapatite filler (Radiesse®) injection. The diffuse hyperechoic nature of the filler is seen

hyperechoic dots. Later HRUS imaging of PMMA may show some coalescence of echogenic deposits, some showing posterior acoustic shadowing.Adverse sequelae after soft tissue augmentation with dermal fillers are fortunately rare. Early adverse events, less than 2 weeks after injection, including edema, bruising, and allergic reactions, are usually self-limited and resolve without intervention in 7–10 days. Late adverse events such as infection, nodules, biofilm, or pigmentation changes may be manifested months to years after the injection. HRUS has been used to both diagnose the type, amount, and depth of placement of dermal fillers [64]. Romana et al. described the use of HRUS in evaluating 80 patients with both permanent and temporary fillers. They were able to identify and quantify the presence of filler in the soft tissues in 97% of patients [65]. One of the more challenging adverse long-term sequelae of permanent fillers is the late development of nodules. Inflammatory complications of nonresorbable filler injections are thought to be caused by the formation of granulomas. Histologically, granulomas consist of multinucleated foreign body cells, macrophages, and angiogenesis. HRUS evaluation of late filler nodules may reveal a hypoechoic mass with a hyperechoic pseudocapsule. Various treatments have been suggested for late post filler injection granulomas including intralesional steroids and injections of 5 flouro-uracil. Cassuto et al. described using HRUS to differentiate late nodules into 2 separate categories [66]. Cystic nodules caused by bolus injections were treated with intralesional, 808 nm fiber laser and stab wound evacuation, while an infiltrating pattern caused by retrograde crisscross injection techniques were treated with intralesional fiber laser alone. Seok et al. described treating late nodules caused by injections of L poly lactic acid fillers with HRUS directed curettage [67]. HRUS can also be used to directly target injection of steroids or 5-fluoro-uracil into the offending mass.

One of the more dreaded complications of soft tissue filler injections of the face is the occlusion of arterial vessels leading to ischemic necrosis of skin and blindness. As there has been a worldwide increase in the use of fillers for cosmetic enhancement of the aging face, the adverse events of ischemic necrosis of soft tissues and blindness have more frequently been reported. HA is the most widely used filler for facial rejuvenation. Unlike the permanent fillers, HA filler effect can be reversed by enzymatic degradation with the injection of hyaluronidase (Hylenex®, Halozyme Therapeutics, San Diego, CA). Hyaluronidase functions as a spreading factor, breaking the glycosidic bonds of the HA inducing depolymerization. In the cases where impending ischemic necrosis of soft tissue is suspected after filler injections, hyaluronidase injection is the treatment of choice. Hyaluronidase is able to penetrate the thin vessel walls and gain access to the HA. One of the leading treatment algorithms for the use of hyaluronidase for impending soft tissue necrosis involves the use of pulsed high-dose injections of hyaluronidase at hourly intervals until the signs of ischemia have been reversed [68]. The empiric nature of this approach and the time involvement of both physician and patient have made this method difficult to employ. Because the amount of injected filler and the precise location of the vessel obstruction are not elucidated in this technique, the final amount of hyaluronidase injected may approach toxic amounts. Schelke et al described the use of Doppler ultrasound to demonstrate a change in the normal laminar flow pattern of unobstructed blood flow to that of a turbulent pattern when

some type of obstruction secondary to the filler exists [69]. Under ultrasound guidance, 35–50 units of hyaluronidase were injected directly into the obstructing filler with resolution of the ischemia in 14 of 21 patients after a single dose. Seven patients required a second treatment. In comparison to the hourly, blind injection pulsed therapy regimen, ultrasound-guided hyaluronidase treatment required less time to administer and less volume of hyaluronidase administered.

One of the newer described uses of CaHA is a hyperdilution technique. CaHa, when used undiluted, acts first by volume enhancement due to the carboxymethylcellulose gel component of the filler. The late-volume enhancement is through biostimulation with the production of collagen, elastin, dermal cell proliferation, and angiogenesis leading to duration of effect of 9–18 months. When CaHa is diluted (1.5 mL CaHA with 1.5 mL or more of sterile saline), the immediate volume correction of the hydrogel is minimized, and the product can be injected more superficially to improve skin quality and thickness. One of the off-label uses of dilute CaHA injection is to improve fine wrinkles, skin texture, and skin tightening of the neck and décolletage. When a cannula injection technique is used, HRUS can be used to visualize the correct plane of filler placement as close to the subdermis as possible. Post injection ultrasound imaging can confirm homogeneous dispersion of the filler.

13.15 DVT

One of the more dreaded complications of plastic surgical procedures is deep vein thrombosis (DVT) and the possibility of subsequent pulmonary embolus (PE). One of the accepted methods of risk assessment for thromboembolism is the application of the Caprini score in the decision-making process for chemoprophylaxis [70, 71]. Several studies have disputed the validity of the Caprini scores showing that it was not predictive of which patients would best be served by chemoprophylaxis [72, 73]. Swanson reported on 1000 consecutive cosmetic plastic surgery patients who underwent screening Doppler ultrasound examination of the lower extremities preoperatively, the day after surgery and 1-week post operatively [74].

Compression, longitudinal color flow and waveform analysis were included. Ultrasound image of DVT shows lack of Doppler blood flow in lower extremity veins. Resolution of clot with restoration of Doppler blood flow is visualized weeks later. Nine patients developed DVT and 1 patient had a PE. Eight of the 9 patients were treated successfully with oral anticoagulants. One patient with PE required hospitalization. No patients were anticoagulated prophylactically. Hematoma formation in anticoagulated patients having abdominoplasty is higher than those patients not having anticoagulation. Ultrasound surveillance can obviate the need for chemo prophylactic anticoagulation of plastic surgery patients thought to be at a higher risk for DVT and possible PE.

13.16 Ultrasound of Soft Tissues

Plastic surgeons regularly diagnose and treat soft tissue masses and are involved in evaluating superficial soft tissue irregularities. Common causes of soft tissue masses include seroma, fat necrosis, benign tumors, inclusion cysts, and foreign bodies. Ultrasound evaluation of soft tissue masses by the plastic surgeon has several advantages. Ultrasound can be readily available at the time of consultation, lacks ionizing radiation, is cost effective, and has high spatial resolution. Ultrasound can also be used to assess blood flow without the necessity for contrast administration. Ultrasound is useful for subcutaneous masses that are more superficial and smaller in size. Deep, large, and subfascial masses are best evaluated with MRI. History from the patient as far as the date the mass was first found, change in size, prior trauma or surgery and associated pain is first elicited. Physical examination can assess mobility, tenderness, firmness, and evaluate overlying changes in the skin. A linear, high-frequency probe is used with the highest frequency possible that will allow

visualization of the deep aspect of the mass as it relates to the soft tissues. Typically, 2–3 cm of depth will be adequate. Lower frequencies may be needed to assess soft tissue masses in the obese patient or in locations with significant adiposity. Doppler ultrasound can be useful in assessment of soft tissue masses. As many soft tissue masses are hypo vascular, detection of slow blood flow will necessitate higher frequency transducers and the use of presets for detection of slow blood flow. It is helpful to both minimize the size of the doppler box to maximize frame rate and to decrease the color Doppler scale to best visualize blood flow. The transducer is floated over the skin with minimal pressure to decrease movement artifacts. Increasing the Doppler gain is done until slow flow is seen. In the event of no visible flow, some artifact in the periphery of the image may be seen.

Lipomas are the most frequently seen benign soft tissue tumor. In one series, lipomas represented 54% of superficial masses sent for ultrasound evaluation over a 3-year period [75]. Ultrasound images of lipomas will frequently appear isoechoic, hyperechoic, or hypoechoic to the surrounding normal fat (Fig. 13.35)

In the series referred to previously, 59% of the masses were isoechoic, 26% hyperechoic, and 15% hypoechoic to the surrounding normal fat [75]. There may be some wavy echogenic lines within the mass. There is minimal to no Doppler signal and no acoustic shadowing is seen. One variant of the lipoma is the angiolipoma, which can be tender to palpation. The ultrasound image of an angiolipoma is homogeneously hyperechoic and will lack the echogenic lines seen in the lipoma.

Soft tissue infections are often evaluated by plastic surgeons. Whether due to a previous surgery, trauma, or other reasons, plastic surgeons need to differentiate cellulitis from abscess (Fig. 13.36).

Ultrasound has been shown to be an excellent tool to aid in this distinction. The ultrasound appearance of cellulitis is that of an expansion of the subcutaneous space with a diffuse hyperechoic nature of the fat. Noninfectious edema of the soft tissues looks similar on ultrasound to that of cellulitis. Ultrasound images of a soft tissue abscess can be diffuse or well circumscribed. There is a surrounding hyperechoic area and may contain poorly defined pockets of hypoechoic spaces. With compression of the abscess, real-time visualization of mobility of the fluid is diagnostic of an abscess. Anechoic pockets of air within the abscess cavity suggest a diagnosis of necrotizing fasciitis.

Fat necrosis presents as a tender firm mass in the superficial soft tissue space. Plastic surgeons will encounter fat necrosis after procedures where ischemia of tissues can be the causative factor. Free and pedicle flap transfers, breast

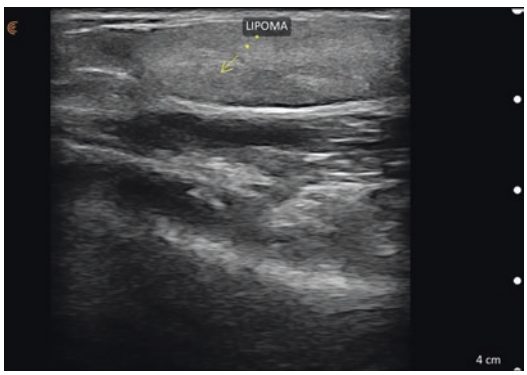

Fig. 13.35 Grayscale ultrasound image of lateral arm. Longitudinal orientation of the transducer over the lateral distal arm shows the well demarcated, homogeneous hyperechoic nature of the lipoma

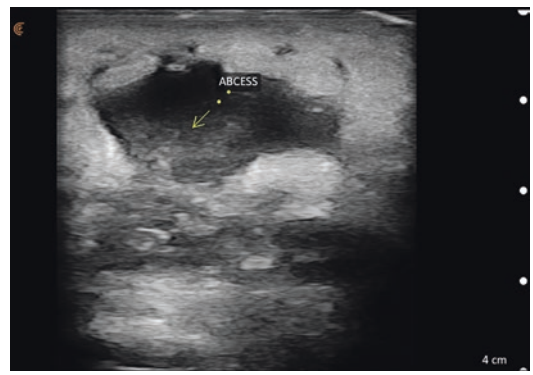

Fig. 13.36 Grayscale ultrasound image of medial knee showing an abscess. The hyperechoic edematous soft tissue surrounds a mostly anechoic chamber with internal debris echoes

reductions, and fat grafting are common causes of fat necrosis. Ultrasound can be used to diagnose and aid in the following clinical course of these benign masses as they tend to resolve without intervention over time. Ultrasound images of fat necrosis can be from isoechoic to hyperechoic to the surrounding normal fat. Anechoic to hypoechoic areas within the mass represent oil cysts (Fig 13.37).

Foreign bodies can present as soft tissue masses. Ultrasound is useful to both diagnose the etiology of and depth of the foreign body and may aid in intraoperatively locating it. Plastic surgeons will on occasion use permanent nonabsorbable sutures made of polypropylene, nylon, polytetrafluorethylene, (PTFE), silk, and polyester. These sutures can develop suture abscesses months to years later and present as soft tissue masses. Ultrasound imaging of suture abscesses reveals the suture material to be hyperechoic with a surrounding area of a hypoechoic halo representing chronic granulation tissue (Fig 13.38).

There may be some posterior acoustic shadowing behind the suture material. Using small skin incisions over the offending suture abscess, ultrasound used intraoperatively can aid in removal of the suture with minimal tissue trauma to the surrounding area.

In plastic surgery patients requesting body contour enhancement procedures such as abdominoplasty and trunk liposuction, ultrasound may be useful in the preoperative evaluation of the anterior abdomen. Occult hernias of the abdominal wall may be difficult to palpate in the patient with a high BMI. Ultrasound can be used in the upright position or with the addition of the Valsalva maneuver to assess the integrity of the anterior abdominal wall. Ventral, epigastric, and spigelian hernias are the most common locations. With the linear, high-frequency transducer placed over the midline or lateral rectus abdominis border, the abdominal wall can be evaluated as the patient does a Valsalva maneuver. Preperitoneal fat, small or large bowel contents may be seen to emanate through the fascial opening. This can be differentiated from the postpartum change of the female abdominal wall where there is an attenuation of the linea aspera of the rectus abdominis, but no true hernia opening is present.

Ultrasound can be useful in detecting hematoma in the post-surgical or post traumatic presentation of acute swelling. The differentiation between edema and blood can be important in dictating whether surgical intervention will be

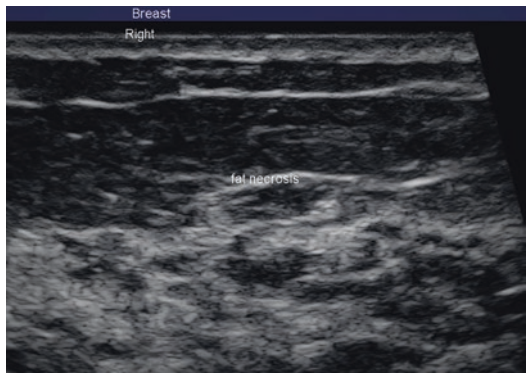

Fig. 13.37 Grayscale ultrasound image of breast showing the diffuse hyperechoic areas with areas of relatively anechoic chambers representing a more liquid oil cyst

Fig. 13.38 Grayscale ultrasound image of anterior abdominal wall showing a hyperechoic mass representing the suture. The anechoic area surrounding the suture represents the chronic granulation tissue. Acoustic shadowing from the suture is seen deep to the suture

necessary. In the acute phase, hematoma can appear hyperechoic on ultrasound. Hematomas, by the time they are evaluated by the plastic surgeon using ultrasound, will usually appear as hypoechoic with some linear hyperechoic lines. As clot retraction liquifies the semi solid blood, the ultrasound appearance will change to an anechoic fluid like appearance.

13.17 Cellulite

Cellulite is one of the most common undesired alterations in the topical appearance of the skin of the posterolateral thigh and buttock. It is much more common in women and affects 85–98% of women at some point in their life [76]. There are a multitude of theoretical causes of cellulite including accumulation of toxins in the hypodermis, obesity, changes in the microcirculation, genetic predisposition, and structural alterations in the relationship of the fibrous septa to the dermis. The dermal and hypodermal architecture of the male and female differ in the orientation and number of septa that attach the fascia to the overlying dermis. In the male, there are numerous septa emanating from the deep fascia in a criss-cross fashion. There is only one fat compartment between the muscle and skin. The female architecture is different in that there is a superficial and deep fat compartment separated by a fascial layer. There are fewer septa, and they tend to be more vertically oriented. HRUS can be used by the plastic surgeon to assess the pathology of cellulite, aid in planning its treatment, and provide documented visual ultrasonic evidence of treatment progress. A linear high-frequency probe (10–15 MHz) is used. In the image of the male and female patient, when the probe is oriented along the long axis of the leg, the muscle of the thigh appears slightly echogenic with visible striations. The fascia and septa are more echogenic lines easily visualized between the muscle fascia and dermis. In the absence of cellulite, there is a constant distance between the fascia and the dermis. Where the dimples and orange peel quality of the skin are evident, the superficial fascia undulates upward toward the dermis, and there is usually a visualized septae at the apex of the upward arc. At the skin hypodermis junction, fat can be seen herniating upward into the dermis. Numerous noninvasive as well as invasive treatments for cellulite have been described. Topical application of aminophylline and retinols have been described as having modest success in reduction in the appearance of cellulite [77, 78]. Injected lipolytic agents such as phosphatidylcholine and deoxycholic acid have been used in mesotherapy treatment of cellulite [79, 80]. High-frequency ultrasound has been used to demonstrate the efficacy of mesotherapy, topical creams, and electro-mechanical massage in the reduction of cellulite. Mechanical vacuum-assisted massage with the addition of heat in the form of lasers or radiofrequency devices have also been described as being effective in temporary reduction in the appearance of cellulite [81–83]. Invasive procedures utilizing fiber laser delivery of energy directed at the fibrous septa thought to be causative of the dimpled appearance of cellulite have been described [84]. Using wavelengths of 1440 nm, a side firing, 1000-μm fiber encased within a hollow cannula was used to treat patients with cellulite of the thighs. A high-frequency linear probe was used to measure dermal thickness. Serial ultrasound images demonstrated an increased thickness of the dermis and a more homogeneous appearance of the dermal–epidermal junction.

13.18 Evaluation of Flaps

For the repair of complex soft tissue defects of the torso, extremities, and face, plastic surgeons have relied upon the use of both pedicled and free tissue transfer of muscle flaps with or without the overlying skin as a primary reconstructive option. Lack of availability of donor site muscle, high donor site muscle morbidity, or requirement of less bulky tissue corrections have led to the increased use of fasciocutaneous flaps as a viable alternative to musculocutaneous flaps. Because of the anatomic variability of the perforating vessels of the fasciocutaneous flaps, several presurgical imaging techniques have been

suggested as being useful in locating these fasciocutaneous perforators. Color Doppler ultrasound (CDU), computed topographic angiography (CTA), and magnetic resonance angiography have all been suggested as viable options for preoperative planning of fasciocutaneous flaps (Fig 13.39).

The deep inferior epigastric perforator flap (DIEP) is one of the more commonly used methods for free flap post mastectomy breast reconstruction. CTA has been shown to be a fast, accurate method of preoperative assessment of the deep inferior epigastric artery (DIEA) showing its intramuscular course and perforator branching pattern as the vessel exits the rectus fascia and enters the subcutaneous tissue [85]. CTA, however, has small risks of contrast toxicity as well as ionizing radiation exposure. Magnetic resonance angiography (MRA) has been shown to be a viable alternative to CTA with no ionizing radiation [86]. MRA image quality may be affected by motion artifact, and the exam may be contraindicated in patients with claustrophobia or ferrous metallic implants [87]. The use of CDU was described by Hallock in the early 1990s in the planning of 8 fasciocutaneous flaps [88, 89]. A 7.5 MHz, linear transducer was used to locate the dominant perforator or perforators in each case. In a comparison study of CDU and CTA, 98 patients underwent 125 DIEP flaps (91). CDU was found to be statistically superior in accuracy of perforator detection and predictor of vessel size compared to CTA.

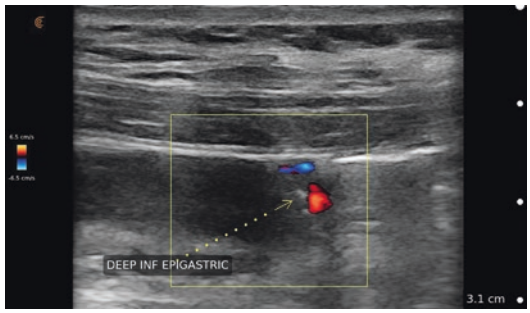

Fig. 13.39 Color Doppler ultrasound image of abdominal wall. Transducer is oriented longitudinally over the rectus muscle below the umbilicus. The deep inferior epigastric artery and vein are seen just below where they enter the rectus abdominis muscle

References

1. American Society of Plastic Surgeons 2018 Cosmetic Plastic Surgery Statistics. American Society of Plastic Surgeons Website.https://www.plasticsurgery.org/documents/News/Statistics/2018/plastic-surgery-statistics report-2018.pdf. Accessed 19 Jan 2020.
2. Cronin T, Gerow F. Augmentation mammoplasty: a new "natural feel" prosthesis. In: Transactions of the third international congress of plastic surgeons. Amsterdam: Excerpta Medica Foundation; 1964. p. 41–9.
3. Ho Lmich LR, Friis S, Fryzek JP, et al. Incidence of silicone breast implant rupture. Arch Surg. 2003;138(7):801e6.
4. Seigle-Murandi F, Lefebvre F, Bruant-Rodier C, Bodin F. Incidence of breast implant rupture in a 12-year retrospective cohort: evidence of quality discrepancy depending on the range. J Plast Reconstr Aesthet Surg. 2017;70(1):42e6.
5. Handel N, Garcia ME, Wixtrom R. Breast implant rupture: causes, incidence, clinical impact, and management. Plast Reconstr Surg. 2013;132(5):1128e37.
6. Kessler DA. Food and Drug Administration. U.S. Department of Health and Human Services. HHS News. No. P92–11. Statement on Silicone Gel Breast Implants. 1992.
7. Food and Drug Administration. Device approvals. 2006. www.fda.gov/MedicalDevices/ProductsandMedicalProcedures/DeviceApprovalsandClearances/Recently-ApprovedDevices/ucm073317.htm.
8. Paetau AA, McLaughlin SA, McNeil RB, et al. Capsular contracture and possible implant rupture: is magnetic resonance imaging useful? Plast Reconstr Surg. 2010;125(3):830e5. FDA General and Plastic Surgery Panel in March, 2019, https://www.fda.gov/media/122960/download.
9. Ikeda DM, Borofsky HB, Herfkens RJ, Sawyer-Glover AM, Birdwell RL, Glover GH. Silicone breast implant rupture: pitfalls of magnetic resonance imaging and relative efficacy of magnetic resonance, mammography, and ultrasound. Plast Reconstr Surg. 1999;104:2054e62.
10. O'Toole M, Caskey CI. Imaging spectrum of breast implants complications: mammography, ultrasound, and magnetic resonance imaging. Semin Ultrasound CT MR. 2000;21:351e61.
11. Di Benedetto G, Cecchini S, Grassetti L, et al. Comparative study of breast implant rupture using mammography, sonography, and magnetic resonance imaging correlation with surgical findings. Breast J. 2008;14(6):532e7.
12. Berg WA, Caskey CI, Hamper UM, et al. Diagnosing breast implant rupture with MR imaging, US, and mammography. Radiographics. 1993;13:1323–36.
13. Scaranelo AM, Marques AF, Smialowski EB, et al. Evaluation of the rupture of silicone breast implants by mammography, ultrasonography and magnetic

resonance imaging in asymptomatic patients: correlation with surgical findings. Sao Paulo Med J. 2004;122(2):41e7.
14. Brown SL, Middleton MS, Berg WA, Soo MS, Pennello G. Prevalence of rupture of silicone gel breast implants revealed on MR imaging in a population of women in Birmingham, Alabama. AJR Am J Roentgenol. 2000;175(4):1057–64.
15. Destouet JM, Monsees BS, Oser RF, Nemecek JR, Young VL, Pilgram TK. Screening mammography in 350 women with breast implants: prevalence and findings of implant complications. AJR Am J Roentgenol. 1992;159(5):973–978; discussion 979–981.
16. Middleton MS. MR evaluation of breast implants. Radiol Clin N Am. 2014;52(3):591–608.
17. Everson LI, Parantainen H, Detlie T, et al. Diagnosis of breast implant rupture: imaging findings and relative efficacies of imaging techniques. AJR Am J Roentgenol. 1994;163(1):57–60.
18. Berg WA, Caskey CI, Hamper UM, et al. Single- and double-lumen silicone breast implant integrity: prospective evaluation of MR and US criteria. Radiology. 1995;197(1):45–52.
19. Rietjens M, Villa G, Toesca A, et al. Appropriate use of magnetic resonance imaging and ultrasound to detect early silicone gel breast implant rupture in postmastectomy recon struction. Plast Reconstr Surg. 2014;134(1):13e–20e.
20. Venta LA, Salomon CG, Flisak ME, Venta ER, Izquierdo R, Angelats J. Sonographic signs of breast implant rupture. AJR Am J Roentgenol. 1996;166(6):1413–9.
21. Chung KC, Malay S, Shauver MJ, Kim HM. Economic analysis of screening strategies for rupture of silicone gel breast implants. Plast Reconstr Surg. 2012;130(1):225–37.
22. Stavros AT. Breast ultrasound. Philadelphia, PA: Lippincott Williams & Wilkins; 2004. p. 199–275.
23. Caskey CI, Berg WA, Anderson ND, Sheth S, Chang BW, Hamper UM. Breast implant rupture: diagnosis with US. Radiology. 1994;190(3):819–23.
24. Robinson OG Jr, Bradley EL, Wilson DS. Analysis of explanted silicone implants: a report of 300 patients. Ann Plast Surg. 1995;34:1e6.
25. US Food and Drug Administration data. http://www.fda.gov/MedicalDevices/ProductsandMedicalProcedures/ImplantsandProsthetics/BreastImplants/ucm063871.html. Accessed 18 Jan 2020.
26. DeBruhl ND, Gorczyca DP, Ahn CY, Shaw WW, Bassett LW. Silicone breast implants: US evaluation. Radiology. 1993;189(1):95–8.
27. Juanpere S, Perez E, Huc O, et al. Imaging of breast implantsda pictorial review. Insights Imaging. 2011;2:653e70.
28. Papadia A, Menada MV, Ragni N, et al. Extended field of view and three dimensional ultrasound imaging of silicone breast implant lesions. Ultrasound Obstet Gynecol. 2007;29:360–1.
29. Sastre G, Rojas R, Roja R, et al. Revisión de implantes mamarios con metodología mamográfica y ultrasonográfica. Rev Argent Radiol. 2005;69:107–12.
30. Gori R. Evaluación ultrasonográfica de la mama con implantes. Rev Argent Ultrason. 2007;6:273–8.
31. Sagi L, Lyakhovitsky A, Barzilai A, et al. Silicone breast implant rupture presenting as bilateral nodules. Clin Exp Dermatol. 2009;34:99–101.
32. Palmon LU, Foshager MC, Parantainen H, et al. Ruptured or intact: what can linear echoes within silicone breast implants tell us? AJR am J Roentgenol. 1997;168:1595–8.
33. Ahn CY, DeBruhl ND, Gorczyca DP, et al. comparative silicone breast implant evaluation using mammography, sonography, and magnetic resonance imaging: experience with 59 implants. Plast Reconstr Surg. 1994;94:620–7.
34. Harris K, Ganott M, Shestak K, et al. Silicone implant rupture: detection with US. Radiology. 1993;187:761–8.
35. Soo MS, Kornguth PJ, Walsh R, et al. Complex radial folds versus subtle signs of intra-capsular rupture of breast implants. MR findings with surgical correlation. AJR Am J Roentgenol. 1996;166:1421e7.
36. Soo MS, Kornguth PJ, Walsh R, et al. Intracapsular implant rupture: MR findings of incomplete shell collapse. J Magn Reson Imaging. 1997;7:724–30.
37. Chung KC, Greenfield ML, Walters M. Decision-analysis methodology in the work-up of women with suspected silicone breast implant rupture. Plast Reconstr Surg. 1998;102:689–95.
38. McNamara M Jr, Middleton M. Ultrasound of breast implants and soft tissue silicone. Ultrasound Clin. 2011;6:345–68.
39. Huch RA, Kunzi W, Debatin JF, et al. MR imaging of the augmented breast. Eur Radiol. 1998;8:371–6.
40. Hold P, Shabana A, Pilbrow W, et al. How should we investigate breast implant rupture. Breast J. 2012;18:253–6.
41. Galdiero M, Larocca F, Iovene MR, et al. Microbial evaluation in capsular contracture of breast implants. Plast Reconstr Surg. 2018;141(1):23–30. https://doi.org/10.1097/PRS.0000000000003915.
42. Wan D, Rohrich RJ. Revisiting the Management of Capsular Contracture in breast augmentation: a systematic review. Plast Reconstr Surg. 2016;137(3):826–41. https://doi.org/10.1097/01.prs.0000480095.23356.ae.
43. Baker JL Jr. Augmentation mammaplasty. In: Owsley Jr JQ, Peterson RA, editors. Symposium on aesthetic surgery of the breast. St Louis: Mosby; 1979.
44. McGuire P, Reisman NR, Murphy DK. Risk factor analysis for capsular contracture, malposition, and late seroma in subjects receiving Natrelle 410 form-stable silicone breast implants. Plast Reconstr Surg. 2017;139:1–9.
45. Adrada BE, Miranda RN, Rauch GM, et al. Breast implant-associated anaplastic large cell lymphoma: sensitivity, specificity, and findings of imaging

studies in 44 patients. Breast Cancer Res Treat. 2014;147:1–14.
46. Mazzocchi M, Dessy LA, Marchetti F, Marchetti F, Carlesimo B. The use of the veress needle to drain mammary periprosthetic fluid. In Vivo. 2010;24(2):219–22.
47. Becker H, Klimczak J. Aspiration of periprosthetic seromas using the blunt SeromaCath. Plast Reconstr Surg. 2016;137(2):473–5. https://doi.org/10.1097/01.prs.0000475795.84725.c4.
48. Blanco R. The 'pecs block': a novel technique for providing analgesia after breast surgery: correspondence. Anaesthesia. 2011;66(9):847–8. https://doi.org/10.1111/j.1365-2044.2011.06838.x.
49. Pérez MF, Duany O, de la Torre PA. Redefining PECS blocks for postmastectomy analgesia. Reg Anesth Pain Med. 2015;40(6):729–30. https://doi.org/10.1097/AAP.0000000000000243.
50. Hebbard P, Fujiwara Y, Shibata Y, Royse C. Ultrasound-guided transversus abdominis plane (TAP) block. Anaesth Intensive Care. 2007;35:616–7.
51. Matsumoto M, Flores EM, Kimachi PP, et al. Benefts in radical mastectomy protocol: a randomized trial evaluating the use of regional anesthesia. Sci Rep. 2018;8:7815.
52. Wang K, Zhang X, Zhang T, et al. The efficacy of ultrasound-guided type ii pectoral nerve blocks in perioperative pain management for immediate reconstruction after modified radical mastectomy: a prospective, randomized study. Clin J Pain. 2018;34:231–6.
53. Bashandy GM, Abbas DN. Pectoral nerves I and II blocks in multimodal analgesia for breast cancer surgery: a randomized clinical trial. Reg Anesth Pain Med. 2015;40:68–74.
54. Neuber F. Fat transplantation report on the negotiations of the Deutscht Gesellsch Chir. Zentralblatt fur Surgery. 1893;22:66.
55. Fiala T. Transversus abdominis plane block during abdominoplasty to improve postoperative patient comfort. Aesthet Surg J. 2015;35:72–80.
56. Sforza M, Andjelkov K, Zaccheddu R, Nagi H, Colic M. Transversus abdominis plane block anesthesia in abdominoplasties. Plast Reconstr Surg. 2011;128:529–35.
57. Cansancao AL, Condé-Green A, Vidigal RA, Rodriguez RL, D'Amico RA. Real-time ultrasound–assisted gluteal fat grafting. Plast Reconst Surg. 2018;142(2):372–6. https://doi.org/10.1097/PRS.0000000000004602.
58. Mofid MM, Teitelbaum S, Suissa D, et al. Report on mortality from gluteal fat grafting: Recommendations from the ASERF task force. Aesthet Surg J. 2017;37:796–806.
59. Cárdenas-Camarena L, Bayter JE, Aguirre-Serrano H, Cuenca-Pardo J. Deaths caused by gluteal lipoinjection: what are we doing wrong? Plast Reconstr Surg. 2015;136:58–66.
60. Cárdenas-Camarena L, Durán H, Robles-Cervantes JA, et al. Critical differences between microscopic (MIFE) and macroscopic (MAFE) fat embolism during liposuction and gluteal lipoinjection. Plast Reconstr Surg. 2018;141:880–90.
61. American Society of Plastic Surgeons. Gluteal fat grafting advisory. https://www.plasticsurgery.org/for-medical-professionals/advocacy/key-issues/gluteal-fatgrafting-advisory. Accessed 31 Jan 2018.
62. Salibian AA, Frey JD, Thanik VD, Karp NS, Choi M. Transversus abdominis plane blocks in microsurgical breast reconstruction: analysis of pain, narcotic consumption, length of stay, and cost. Plast Reconstr Surg. 2018;142(3):252e–63e. https://doi.org/10.1097/PRS.0000000000004632.
63. Cassuto D, Pignatti M, Pacchioni L, Boscaini G, Spaggiari A, De Santis G. Management of complications caused by permanent fillers in the face: a treatment algorithm. Plast Reconstr Surg. 2016;138(2):215e–27e. https://doi.org/10.1097/PRS.0000000000005203.
64. Grippaudo FR, Mattei M. The utility of high-frequency ultrasound in dermal filler evaluation. Ann Plast Surg. 2011;67(5):469–73. https://doi.org/10.1097/SAP.0b013e318203ebf6.
65. Cassuto D, Pignatti M, Pacchioni L, Boscaini G, Spaggiari A, De Santis G. Management of complications caused by permanent fillers in the face: a treatment algorithm. Plast Reconstr Surg. 2016;138(2):215e–27e. https://doi.org/10.1097/PRS.0000000000002350.
66. DeLorenzi C. New high dose pulsed hyaluronidase protocol for hyaluronic acid filler vascular adverse events. Aesthet Surg J. 2017;37:1–12.
67. Wagner JM, Lee KS, Rosas H, et al. Accuracy of sonographic diagnosis of superficial masses. J Ultrasound Med. 2013;32(8):1443–50.
68. Schelke LW, Velthuis P, Kadouch J, Swift A. Early ultrasound for diagnosis and treatment of vascular adverse events with hyaluronic acid fillers. J Am Acad Dermatol. 2019;88:79. https://doi.org/10.1016/j.jaad.2019.07.032.
69. Murphy RX Jr, Alderman A, Gutowski K, et al. Evidence-based practices for thromboembolism prevention: summary of the ASPS venous thromboembolism task force report. Plast Reconstr Surg. 2012;130:168e–75e.
70. Pannucci CJ, Barta RJ, Portschy PR, et al. Assessment of post-operative venous thromboembolism risk in plastic surgery patients using the 2005 and 2010 Caprini risk score. Plast Reconstr Surg. 2012;130:343–53.
71. Swanson E. Caprini scores, risk stratification, and rivaroxaban in plastic surgery: time to reconsider our strategy. Plast Reconstr Surg Glob Open. 2016;4:e733.
72. Keyes GR, Singer R, Iverson RE, Nahai F. Incidence and predictors of venous thromboembolism in abdominoplasty. Aesthet Surg J. 2018;38:162–73.
73. Swanson E. Prospective study of doppler ultrasound surveillance for deep venous thromboses in 1000 plastic surgery outpatients. Plast Reconstr

Surgery. 2020;145(1):85–96. https://doi.org/10.1097/PRS.0000000000006343.
74. Seok J, Kim JM, Kwon TR, Kim JH, Li K, Kim BJ. Ultrasonography-guided curettage of polyDL-lactic acid filler granulomas. J Am Acad Dermatol. 2018;78(1):e5–6. https://doi.org/10.1016/j.jaad.2017.08.026.
75. Khan MH, Victor F, Rao B, Sadick NS. Treatment of cellulite: part I. pathophysiology. J Am Acad Dermatol. 2010;62(3):361–70.
76. Kligman AM, Pagnoni A, Stoudemayer T. Topical retinol improves cellulite. J Dermatol Treat. 1999;10:119–25.
77. Collis N, Elliot LA, Sharpe C, Sharpe DT. Cellulite treatment: a myth or reality: a prospective randomized, controlled trial of two therapies, endermologie and aminophylline cream. Plast Reconstr Surg. 1999;104:1110–4.
78. Palmer M, Curran J, Bowler P. Clinical experience and safety using phosphatidylcholine injections for the localized reduction of subcutaneous fat: a multicentre, retrospective UK study. J Cosmet Dermatol. 2006;5:218–26.
79. Rotunda AM, Suzuki H, Moy RI, et al. Detergent effects of sodium deoxycholate are a major feature of an injectable phosphatidylcholine formulation used for localized fat dissolution. Dermatol Surg. 2004;30:1001–7.
80. Alster TS, Tanzi EL. Cellulite treatment using a novel combination radiofrequency, infrared light, and mechanical tissue manipulation device. J Cosmet Laser Ther. 2005;7:81–5.
81. Sadick N, Magro C. a study evaluating the safety and efficacy of the VelaSmooth system in the treatment of cellulite. J Cosmet Laser Ther. 2007;9:15–20.
82. Kulick M. Evaluation of the combination of radiofrequency, infrared energy, and mechanical rollers with suction to improve skin surface irregularities (cellulite) in a limited treatment area. J Cosmet Laser Ther. 2006;8:185–90.
83. DiBernardo BE. Treatment of cellulite using a 1,440-nm pulsed laser with one-year followup. Aesthet Surg J. 2011;31:328–41.
84. Cina A, Salgarello M, Barone-Adesi L, Rinaldi P, Bonomo L. Planning breast reconstruction with deep inferior epigastric artery perforating vessels: multidetector CT angiography versus color doppler US. Radiology. 2010;255(3):979–87. https://doi.org/10.1148/radiol.10091166.
85. Cina A, Barone-Adesi L, Rinaldi P, et al. Planning deep inferior epigastric perforator flaps for breast reconstruction: a comparison between multidetector computed tomography and magnetic resonance angiography. Eur Radiol. 2013;23(8):2333–43. https://doi.org/10.1007/s00330-013-2834-x.
86. Schaverien MV, Ludman CN, Neil-Dwyer J, McCulley SJ. Contrast-enhanced magnetic resonance angiography for preoperative imaging of deep inferior epigastric artery perforator flaps: advantages and disadvantages compared with computed tomography angiography: a United Kingdom perspective. Ann Plast Surg. 2011;67(6):671–4. https://doi.org/10.1097/SAP.0b013e3181fab9ea.
87. Hallock GG. Evaluation of fasciocutaneous perforators using color duplex imaging. Plast Reconstr Surg. 1994;94(5):644–51. https://doi.org/10.1097/00006534-199410000-00012.
88. Mijuskovic B, Tremp M, Heimer MM, et al. color doppler ultrasound and computed tomographic angiography for perforator mapping in DIEP flap breast reconstruction revisited: a cohort study. J Plast Reconstr Aesthet Surg. 2019;72(10):1632–9. https://doi.org/10.1016/j.bjps.2019.06.008.
89. Wortsman X, Wortsman J, Orlandi C, Cardenas G, Sazunic I, Jemec GBE. Ultrasound detection and identification of cosmetic fillers in the skin: ultrasound of fillers complications. J Eur Acad Dermatol Venereol. 2012;26(3):292–301. https://doi.org/10.1111/j.1468-3083.2011.04047.x.